How to Cite:
Rao, R. S. D., Vijayakumar, R., & Murthy, V. V. (2022). Numerical study of Casson-Nanofluid flow past an exponentially stretching sheet filled by porous medium in presence of velocity and thermal slip effects. *International Journal of Health Sciences*, *6*(S6), 2695–2725. https://doi.org/10.53730/ijhs.v6nS6.9913

Numerical study of Casson-Nanofluid flow past an exponentially stretching sheet filled by porous medium in presence of velocity and thermal slip effects

R. S. Durga Rao
Department of Mathematics, Vishnu Institute of Technology, Bhimavaram, West Godavari (Dt), 534201, Andhra Pradesh, India
Email: durgarao.r@vishnu.edu.in

R. Vijayakumar
Mathematics Section, FEAT, Annamalai University, Chidambaram, Tamilnadu State, India | Department of Mathematics, Periyar Government Arts College, Cuddalore, 607001, Tamilnadu State, India
*Corresponding author email: vijayakumar@pacc.in

V. Vasudeva Murthy
Department of Mathematics, S. R. K. R. Engineering College, Bhimavaram, West Godavari (Dt), 534201, Andhra Pradesh, India

***Abstract*---**An inquiry of the non-Newtonian Casson flow of nanofluid through a non-linear exponentially expanding sheet is one of the things that will be covered in the course of this work. When a magnetic field, chemical reaction, thermophoresis, and Brownian motion phenomena are present, the influence of coupled velocity and thermal slip conditions on porous embedded fluid flow is investigated. These phenomena include Brownian motion. In particular, the flow of fluid through porous embedded structures is studied in the presence of a magnetic field. Because the mechanics of fluid motion are extremely sequential and non-linear, fluid dynamics may be described as having these characteristics. In order to acquire an approximate answer, what has been done here is to combine the Runge-Kutta method with a numerical approach that makes use of the shooting technique and a shooting scheme. This has been done in order to get an approximation. The degree to which the thermo-fluid parameters are susceptible to change is shown by both the tabular and graphical representations of the data. When the new findings are contrasted with the findings of the earlier study, there may be found to be a high degree of congruence between the two sets of findings. This finding

Manuscript submitted: 9 March 2022, Manuscript revised: 27 May 2022, Accepted for publication: 18 June 2022

may have applications in a wide variety of different fields, including aviation technology, manufacturing, medical systems, and solar nanofluids systems, to name just a few of those that come to mind immediately. The findings of this research will also contribute to the development of nanotechnology, chemical engineering, and thermal engineering, all of which will benefit from the findings.

***Keywords*---**casson fluid, nanofluid, exponentially stretching sheet, porous medium, velocity slip, thermal slip, thermophoresis, brownian motion.

Nomenclature
List of Symbols

u, v : x and y directions velocity components respectively (m/s)
x, y : Cartesian coordinates calculated along the stretching sheet (m)
f : Dimensionless stream function ($kg/\ m.\ s$)
f' : Fluid velocity (m/s)
Pr : Prandtl number
C : Fluid nanoparticle volume concentration ($mol\ /\ m^3$)
C_∞ : Dimensional ambient volume fraction ($mol\ /\ m^3$)
T : Fluid temperature (K)
C_w : Dimensional nanoparticle concentration at the stretching surface ($mol\ /\ m^3$)
T_w : Surface Temperature (K)
$B(x)$: Magnetic field function ($Tesla$)
B_o : Uniform magnetic field ($Tesla$)
O : Origin
T_∞ : Temperature of the fluid far-off from the stretching sheet (K)
M : Magnetic field parameter
Cf : Skin-friction coefficient (s^{-1})
U_w : Reference velocity (m/s)
Nb : Brownian motion parameter
$u_w(x)$: Stretching velocity of the fluid (m/s)
Nu : Rate of heat transfer coefficient (or)Nusselt number
V_w : Mass transfer velocity (m/s)
Nt : Thermophoresis parameter
Le : Lewis number parameter
q_w : Heat flux coefficient

q_m : Mass flux coefficient
C_p : Nano particles Specific heat capacity $(J / kg / K)$
D_B : Coefficient of Brownian diffusion (m^2 / s)
D_T : Coefficient of Thermophoresis diffusion (m^2 / s)
S : Suction/Injection parameter
Sh : Rate of mass transfer coefficient (or) Sherwood number
K : Permeability parameter (m^{-1})
k_1 : Permeability of porous medium (m^{-1})
L_1 : Velocity Slip length (m)
L_2 : Thermal slip length (m)
a : Positive real number
U_o : Reference velocity (m/s)
Re_x : Reynold's number
R : Thermal radiation parameter
q_r : Dimensional chemical reaction parameter
H : Joule heating parameter
K^* : Mean absorption coefficient
L : Slip length (m)

Greek symbols

γ : Chemical reaction parameter
η : Dimensionless similarity variable (m)
θ : Non-dimensional temperature (K)
ϕ : Non-Dimensional nanoparticle concentration (mol / m^3)
α_m : Thermal diffusivity, (m^2 / s)
ν : Kinematic viscosity, (m^2 / s)
σ : Stefan-Boltzmann constant, $(W . m^{-2}. K^{-4})$
ρ : Fluid density, (kg / m^3)
μ : Dynamic viscosity of the fluid, (*Pascal-second*)
κ : Thermal conductivity of the fluid,$(W / (m{\cdot}K))$
β : Casson fluid parameter
λ : Velocity slip parameter
δ : Thermal slip parameter
τ : Cauchy Stress tensor
μ_B : Casson fluid Dynamic viscosity (m^2/s)
α^* : Shear rate
σ^* : Stefan-Boltzmann constant

τ_w : Shear stress

Superscript

$'$: Differentiation w.r.t η

Subscripts

f : Fluid,
w : Condition on the sheet
∞ : Ambient Conditions.

Introduction

Academics have recently been interested in magnetohydrodynamic (MHD) flow as a result of the many applications it offers in engineering and industry. For instance, the cooling of several continuous strips may be performed in metallurgical processes by drawing electrically conducting fluids that are sensitive to magnetic fields [1]. It makes it possible to manage the pace of cooling, which ultimately produces the desired effects. Another use of hydro-magnetic flow in the realm of metallurgy is the removal of non-metallic impurities from molten metals by using a variety of magnetic field purification techniques. As a consequence of this, a significant number of researchers have focused their attention on the flow and heat transfer of electrically conducting fluids in the presence of magnetic fields, such as liquid metals mixed with acid. Herdricha et al. [2] conducted research on the magnetohydrodynamic flow with the purpose of controlling plasma technology. In this study, they highlighted the possible use of magnetic fields in magnetically controlled plasmas in space field technologies. Casson hybrid nanofluid radiative MHD flow was examined by Veera Krishna et al. [3] over an infinite exponentially accelerated vertical porous surface. Veera Krishna and Chamkha [4] investigated the Hall and ion slip effects on the MHD rotating boundary layer flow of nanofluid via an infinite vertical plate that was embedded in a porous medium. Veera Krishna and Chamkha [5] investigated the Hall and ion slip effects on the MHD rotational flow of an elastico-viscous fluid via porous medium. The effects of MHD flow of second-grade fluid through porous medium on heat and mass transport were studied by Veera Krishna et al. [6] who explored the flow of the fluid through a semi-infinite vertical stretching sheet. The impact of Hall on MHD Veera Krishna and Chamkha [7] examined the flow of a water-based nano fluid being compressed between two parallel discs. Veera Krishna and colleagues [8] investigated heat and mass transfer in free convective flow of a micropolar fluid through a porous surface with an angled magnetic field and Hall phenomena. Veera Krishna and Chamkha [9] looked into the MHD peristaltic rotating flow of a couple stress fluid through a porous medium while taking into account wall and slip effects. Veera Krishna et al. [10] conducted research to examine Hall effects on unsteady MHD oscillatory free convective flow of second grade fluid through porous material between two vertical plates. Veera Krishna and Chamkha [11] looked at the Hall effects of an unsteady MHD flow of a second-grade fluid through porous medium with ramping wall temperature and ramping surface concentration. Veera Krishna and colleagues [12] investigated heat and mass transfer on unsteady, magnetohydrodynamic, oscillatory flow of second-grade fluid through a porous media located between two vertical plates while taking into account the influence of varying heat sources and sinks as well as chemical reactions. Veera Krishna and colleagues [13] conducted research to examine heat and mass transfer on magnetohydrodynamic chemically reacting flow of micropolar fluid through a porous media while accounting for Hall effects.

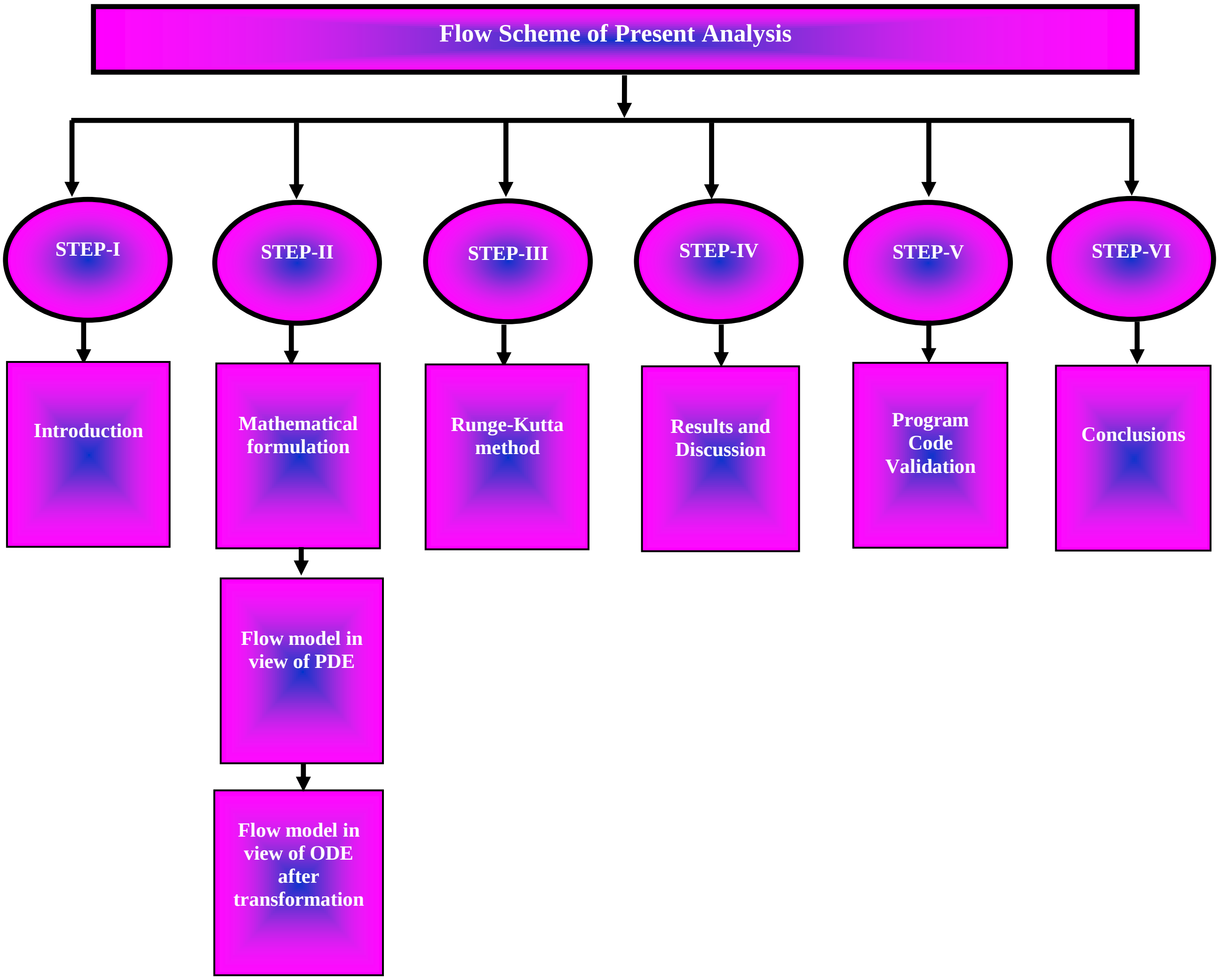

Fig. 1. Design study

Hall effects on MHD were investigated by Veera Krishna et al. [14]. The flow of Jeffrey fluid in a peristaltic motion through porous material in a vertical strata. Hall and ion slip effects were studied by Krishna and Chamkha [15] in their research on the unsteady MHD convective rotating flow of nanofluids. ThameemBasha et al. [16] studied the flow of SWCNH/diamond-ethylene glycol nano-fluid via a wedge, a plate, and a stagnation point using an induced magnetic field and a non-linear radiation-solar energy application. Researchers Kumar et al. [17] looked into how dissipative fluid magneto-convection flow was affected by the influence of produced magnetic fields as well as heat radiation. Analytical modelling was used by Modather et al. [18] in order to explore the oscillatory flow of a micropolar fluid via a vertical permeable plate located in a porous material. The MHD boundary layer flow, heat and mass transfer over a spinning disc in a porous medium saturated with Cu-water and Ag-water nano-fluid was explored by Sudarsana Reddy and colleagues [19]. Ramesh et al. [20] used a permeable cylinder as both a heat source and sink for their study of heat transfer in aluminium alloy and magnetite graphene oxide. Menni et al. [21] studied the hydrodynamics and thermal properties of water, ethylene glycol, and water-ethylene glycol as base fluids distributed by aluminium oxide nano-sized solid particles. When studying the Cattaneo-Christov heat diffusion phenomenon in a Reiner-Philippoff fluid, Ganesh Kumar and colleagues [22] used the usage of a transverse magnetic field in their research. Research conducted over the last several years on boundary layer flow and heat transfer over a linearly stretched plate has shown to be rather valuable due to the fact that it has a wide variety of applications in both the scientific and commercial worlds.

Metal spinning, metal extrusion, glass fibre, wire drawing, hot rolling, artificial fibres, continuous stretching of plastic films, copper wire drawing, and polymer extrusion are just some of the applications that may be found for this material. The Casson nano fluid boundary layer flows, heat transport, and chemical reactions across a stretched surface are the primary focuses of the study being conducted at the moment. A liquid that can move about is referred to as a fluid. A nano fluid consists of a base fluid and nanoparticles mixed together. Nanoparticles may range in size anywhere from one to one hundred nano-meters. The basic fluid is composed of ethylene, glycol, and toluene, all of which have similar properties to water. After this step, the fundamental fluid is converted into the nano fluid by the addition of carbides, metals, oxides, or other compounds that aren't metals. The use of nano fluids is intended to assist in the determination of how the temperature of the liquid changes over time. The incorporation of nanoparticles into the base fluid may result in an increase in the thermal conductivity of nano fluids.

This method of increasing thermal conductivity may be used for a variety of purposes, including the cooling of heat exchanges, the production of double-pane windows, and other tasks. In the motion of a "Casson nanofluid" across a stretched plate, the manner in which heat travels through the fluid plays an extremely significant role. You need to have a solid understanding of the physics behind how heat travels over a stretched plate in order to get the level of quality you want. This is due to the fact that the value of the end product is mostly determined by how well it stretches and how rapidly heat can pass through it. Following the seminal work done by Sakiadis [23], there has been a significant amount of study published on the flow of "Newtonian" and "non-Newtonian" fluids in the boundary layer that is created over a non-linear or linear stretching plate.

The objective of the study carried out by Mamun et al. [24] is to identify a Casson-type of non-Newtonian fluid flow that occurs toward a stretched surface and is accompanied by thermophoresis, radiation absorption, and a periodic hydromagnetic effect. Researchers Shah et al. [25] employed a surface that had been stretched in order to investigate the flow of Casson nano fluid. Additionally, they investigated the amount of energy required to initiate a chemical reaction and the activation energy. In their study, Nayak et al. [26] investigated the significant discoveries that can be made regarding three-dimensional unsteady MHD flow and the entropy generation of micro-polar Casson cross nano-fluid in terms of non-linear heat radiation, chemical reaction, Brownian movement, thermophoresis effect, convective boundary conditions, viscous dissipation, and Joule heating. Rasoola et al. [27] investigated the characteristics of a nano-fluid of the Casson type by forcing it to flow through an absorbent medium and then through a surface that was stretched in a manner that wasn't straight.

They did this in order to see how the properties changed. They accomplished this in order to increase the flow of heat and mass throughout the system. A simulated investigation of Casson nano-liquid over parallel stretching surface with magnetic field and Joule heating with slip and heat convection boundary condition was described in Kamran et al. [28]. When there existed a convective boundary condition, Sulochana et al. [29] obtained numerical solutions for a three-dimensional Casson nanofluid that was created by a permeable stretched sheet. Raza [30] investigated how slip influences the MHD Casson fluid stagnation point flow on a convective stretched sheet with thermal radiation. He did this by using a convective stretched sheet. Using a three-dimensional convective and radiative MHD Casson nanofluid flow, Kumar et al. [31] investigated the flow of the nanofluid across an exponentially accelerating stretched sheet. Ullah et al. [32] investigated the impact of velocity slip on MHD Casson fluid when it was passed over a sheet that was stretched in a manner that was not linear. This was carried out in a material that was porous, and Newtonian heating was taking place. Researchers at Souayeh and colleagues [33] investigated the flow of Casson nanofluids in the presence of nonlinear thermal radiation. Rashidi et al. [34] investigated how heat radiation impacts the flow of a nanofluid over a stretched sheet and how the buoyancy of the nanofluid affects that flow.

With regard to non-Newtonian nanofluid, Shaw and his colleagues ([35] and [36]) investigated the Casson nanofluid flow in conjunction with nonlinear thermal radiation. Gbadeyan et al. [37] employed convective boundary conditions with velocity slip to examine how viscosity and thermal conductivity impact the flow of nanofluids of the Casson type. Their research focused on how these factors affect the flow of nanofluids. Hayat et al. [38] talked about a research that looked at both viscous dissipation and thermophysical effects in a Casson-type nanofluid flow inside of a heavily stretched cylinder. The investigation was conducted in a Casson-type nanofluid flow. In their study, Archana and colleagues [39] investigated the effects of non-linear energy radiation on Casson-nano liquid. Mustafa et al. [40] performed a simulation of a magnetohydrodynamics influence on a Casson nanofluid. Casson nano flow was the subject of investigation by Gireesha et al. [41], who used radiation and a chemical reaction. The Casson nano flow was then given an additional heat release and loss by Jayarami Reddy et al. [42].

The effects of velocity and thermal slip conditions on electrically conducting, incompressible, viscous natural convection flow of Casson nanofluid caused by nonlinearly exponentially stretching sheet through porous medium in the presence of Magnetic field, Chemical reaction, Thermophoresis, and Brownian motion effects are of the utmost importance. This is evidenced by the literature survey that was mentioned previously as well as the numerous engineering and industrial applications that have been implemented. After converting the governing equations to ordinary differential equations with the use of similarity transformations, numerical solutions are found with the help of the shooting approach and the Runge-Kutta method. Using the numerical data, we investigate the variation in wall drag factor, heat and mass transfer rates, and we construct graphs for various progressive values of non-dimensionalized parameters. According to the findings, an increase in the inertial effect leads to a reduction in the momentum boundary layer as well as the resistance that porous medium offers to the flow of fluid. In order to verify and conduct an analysis of the numerical method presented in the approach for the current problem, the findings are compared with the results that are found in the existing literature in a variety of constrained conditions. It is important to note that the results are seen as being in very close agreement with one another. Fig. 1 presents the flow chart that was created for this project.

Flow Governing Equations

The flow characteristics of incompressible, electrically conducting, viscous, steady, two-dimensional Casson-nanofluid flow towards non-linearly stretching sheet filled by porous medium in the presence of Thermophoresis, Brownian motion, Chemical reaction, Joule heating and magnetic field effects. For this flow, the flow geometry is shown in the Fig. 2. For this research work, the following assumptions are considered for this investigation:

- The x-axis is taken along the stretching surface in the direction of motion and the y-axis is perpendicular to it.
- The flow is confined to $y > 0$. Two equal and opposite forces are applied along the x-axis.
- At $y \geq 0$, the boundary-layer takes place where the coordinate is given normally to the stretching surface.
- The steady and convective Casson-nanofluid flow with the boundary layer in the existence of the uniform magnetic field of strength B_o.
- In the present analysis, the nanoparticles are swayed in the base fluid according to the Brownian
- motion and Thermophoresis.
- The nanoparticle volume concentration C and the temperature on the boundaries are taken to be T_w and C_w, at the wall, T_∞ and C_∞, respectively are far-away from the wall.
- It is assumed that sheet is shrink exponentially with velocity $u_w\left(x\right)=U_w \exp\left(\dfrac{x}{L}\right)$,
- It is also consider that the magnetic field B (x) is of the form

$$B = B_o \exp\left(\frac{x}{L}\right), \qquad (1)$$

- For non-Newtonian fluid, the rheological equation is defined as, $\tau = \tau_o + \mu\alpha^*$ (2)
- For Casson fluid, Eq. (1) can be expanded as,
  $\tau_{ij} = \left\{ 2\left(\mu_B + \frac{p_y}{\sqrt{2\pi}}\right)e_{ij},\ \pi > \pi_c \ \ \&\ 2\left(\mu_B + \frac{p_y}{\sqrt{2\pi_c}}\right)e_{ij},\ \pi < \pi_c \right.$
  (3)
- Where $\pi = e_{ij}e_{ji}$ with e_{ij} is the $(i,\ j)^{th}$ component of the fluid deformation rate and $p_y = \frac{\mu_B\sqrt{2\pi}}{\beta}$ is the yield stress of the Casson fluid.

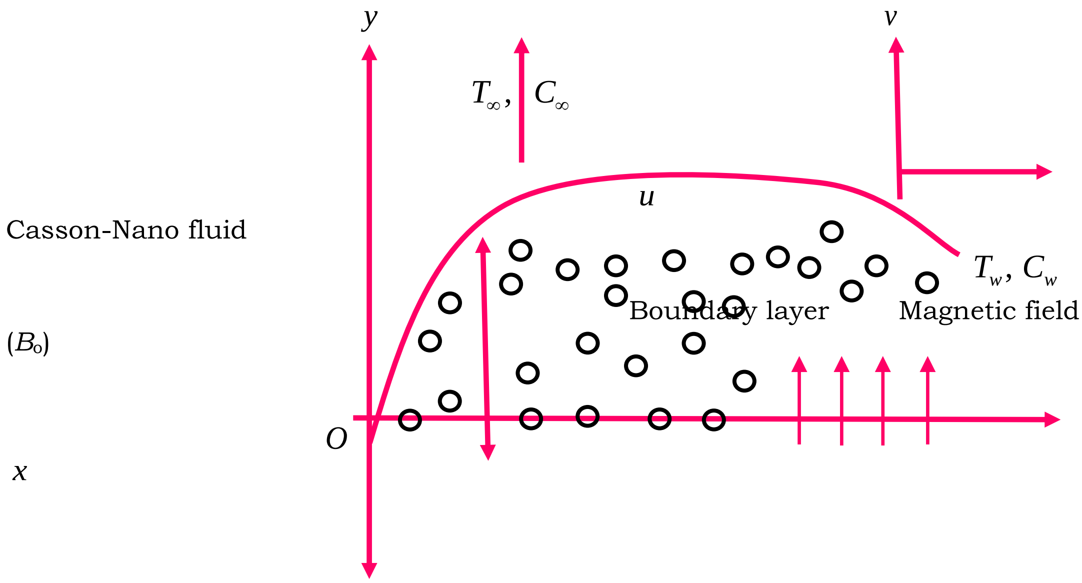

Fig. 2. Geometry representation of the fluid

Based on the above assumptions, the boundary layer equations for steady, two-dimensional, electrically conducting, incompressible, Casson-nanofluid flow are:

Continuity Equation

$$\frac{\partial u}{\partial x} + \frac{\partial v}{\partial y} = 0,$$
(4)

Momentum Equation

$$u\frac{\partial u}{\partial x}+v\frac{\partial u}{\partial y}=\nu\left(1+\frac{1}{\beta}\right)\frac{\partial^2 u}{\partial y^2}-\frac{\sigma B_o^2}{\rho}u-\nu\frac{u}{k_1},$$
(5)

Equation of thermal energy

$$u\frac{\partial T}{\partial x}+v\frac{\partial T}{\partial y}=\alpha_m\frac{\partial^2 T}{\partial y^2}+\tau_B\left\{D_B\frac{\partial C}{\partial y}\frac{\partial T}{\partial y}+\frac{D_T}{T_\infty}\left(\frac{\partial T}{\partial y}\right)^2\right\}-\frac{1}{\rho C_p}\left(\frac{\partial q_r}{\partial y}\right)+\frac{\sigma B_o^2 u^2}{\rho C_p},$$
(6)

Equation of species nanoparticle volume concentration

$$u\frac{\partial C}{\partial x}+v\frac{\partial C}{\partial y}=D_B\frac{\partial^2 C}{\partial y^2}+\frac{D_T}{T_\infty}\frac{\partial^2 T}{\partial y^2}-Kr\left(C-C_\infty\right),$$
(7)

The boundary conditions for this flow are

$$\left.\begin{array}{l} u_w\left(x\right)=U_w\left(x\right)=ax+L_1\left(\frac{\partial u}{\partial y}\right),\ v_w\left(x\right)=-V_w\left(x\right),\ T=T_w+L_2\left(\frac{\partial T}{\partial y}\right),\ C=C_w\ \ at\ \ y=0 \\ u\to 0,\ v\to 0,\ T\to T_\infty,\ C\to C_\infty\ \ as\ \ y\to\infty \end{array}\right\},$$
(8)

The radiative heat flux q_r (using Rosseland approximation (Brewster [43])) is defined as

$$q_r=-\frac{4\sigma^*}{3K^*}\left(\frac{\partial T^4}{\partial y}\right) \qquad (9)$$

We assume that the temperature variances inside the flow are such that the term T^4 can be represented as linear function of temperature. This is accomplished by expanding T^4 in a Taylor series about a free stream temperature T_∞ as follows:

$$T^4=T_\infty^4+4T_\infty^3\left(T-T_\infty\right)+6T_\infty^2\left(T-T_\infty\right)^2+\ldots\ldots\ldots\ldots \qquad (10)$$

After neglecting higher-order terms in the above equation beyond the first degree term in $\left(T-T_\infty\right)$, we get

$$T^4\cong 4T_\infty^3 T-3T_\infty^4 \qquad (11)$$

Thus substituting Eq. (11) in Eq. (9), we get

$$q_r = -\frac{16T_\infty^3\sigma^*}{3K^*}\left(\frac{\partial T}{\partial y}\right) \quad (12)$$

Using (12), Eq. (6) can be written as

$$u\frac{\partial T}{\partial x}+v\frac{\partial T}{\partial y}=\alpha_m\frac{\partial^2 T}{\partial y^2}+\tau_B\left\{D_B\frac{\partial C}{\partial y}\frac{\partial T}{\partial y}+\frac{D_T}{T_\infty}\left(\frac{\partial T}{\partial y}\right)^2\right\}+\frac{1}{\rho C_p}\left(\frac{16T_\infty^3\sigma^*}{3K^*}\right)\left(\frac{\partial^2 T}{\partial y^2}\right)+\frac{\sigma B_o^2u^2}{\rho C_p}, \quad (13)$$

Introducing the following similarity transformations

$$\left.\begin{array}{l} u=U_o\exp\left(\dfrac{x}{L}\right)f'(\eta),\ v=-\sqrt{\dfrac{\nu U_o}{2L}}\exp\left(\dfrac{x}{2L}\right)\left\{f(\eta)+\eta f'(\eta)\right\}, \\ \eta=y\sqrt{\dfrac{U_o}{2\nu L}}\exp\left(\dfrac{x}{2L}\right),\ \ \theta=\dfrac{T-T_\infty}{T_w-T_\infty},\ \ \phi=\dfrac{C-C_\infty}{C_w-C_\infty} \end{array}\right\}, \quad (14)$$

Making the help of Eq. (14), the continuity equation is identically fulfilled and Eqs. (5) to (7) get the subsequent forms are

$$\left(1+\frac{1}{\beta}\right)f'''+ff''-2\left(f'^2\right)-\left(M+K\right)f'=0, \quad (15)$$

$$\left(1+\frac{4R}{3}\right)\theta''+\Pr Nb\theta'\phi'+\Pr Nt\theta'^2+\Pr Hf'^2+\Pr f\theta'=0, \quad (16)$$

$$Nb\phi''+NbLef\phi'+Nt\theta''-Nb\gamma\phi=0, \quad (17)$$

the corresponding boundary conditions (8) become

$$\left.\begin{array}{l} f(0)=S,\ f'(0)=1+\lambda f''(0),\ \theta(0)=1+\delta\theta'(0),\ \phi(0)=1 \\ f'(\infty)\to 0,\ \theta(\infty)\to 0,\ \phi(\infty)\to 0 \end{array}\right\}, \quad (18)$$

where the involved physical parameters are defined as

$$\left.\begin{array}{l} M=\dfrac{\sigma B_o^2}{\rho c},\ \Pr=\dfrac{\nu}{\alpha_m},\ Nb=\dfrac{\tau_B D_B\left(C_w-C_\infty\right)}{\nu},\ S=\dfrac{V_w}{\nu c},\ Le=\dfrac{\nu}{D_B}, \\ Nt=\dfrac{\tau_B D_T\left(T_w-T_\infty\right)}{\nu},\ K=\dfrac{\nu}{ck_1},\ R=\dfrac{4\sigma^* T_\infty^3}{\kappa K^*},\ \gamma=\dfrac{KrU_o\left(C_w-C_\infty\right)}{\nu}, \\ c=\dfrac{U_o e^{\frac{x}{L}}}{2L},\ \lambda=L_1\sqrt{\dfrac{ac}{\nu}},\ \delta=L_2\sqrt{\dfrac{ac}{\nu}},\ H=M.Ec=\dfrac{U_o e^{\frac{x}{L}}}{C_p},\ \mathrm{Re}_x=\dfrac{U_w L}{\nu} \end{array}\right\},$$

Our physical interest of quantities, the physical parameters of the skin-friction coefficient, local Nusselt number and local Sherwood number are presented as follows:

$$Cf=\frac{\tau_w}{\frac{\rho U_w^2}{2}}=\frac{\mu\left(\frac{\partial u}{\partial y}\right)_{y=0}}{\frac{\rho U_w^2}{2}}\Rightarrow\left(\sqrt{\mathrm{Re}_x}\right)Cf=f''(0) \tag{20}$$

$$Nu=\frac{Lq_w}{\kappa\left(T_w-T_\infty\right)}=-\frac{L\kappa\left(\frac{\partial T}{\partial y}+\frac{\partial q_r}{\partial y}\right)_{y=0}}{\left(T_w-T_\infty\right)}\Rightarrow Nu=-\left(1+\frac{4R}{3}\right)\left(\sqrt{\frac{\mathrm{Re}_x}{2}}\right)\theta'(0) \tag{21}$$

$$Sh=\frac{Lq_m}{\kappa\left(C_w-C_\infty\right)}=-\frac{L\left(\frac{\partial C}{\partial y}\right)_{y=0}}{\left(C_w-C_\infty\right)}\Rightarrow Sh=-\left(\sqrt{\frac{\mathrm{Re}_x}{2}}\right)\phi'(0) \tag{22}$$

Method of Solution by Runge-Kutta method:

An exact solution does not seem to be possible in the case of a full set of Eqs. (15)-(17). This is due to the non-linear nature of (15)-(17), with suitable boundary conditions provided in (18) and the need for numerical methods to solve the problem: A similarity transformations are used to turn the governing partial differential equations into a set of non-linear ordinary differential equations that can be numerically solved. The shooting method is used with a fourth-order Runge-Kutta strategy to solve the resulting boundary value issue numerically. A collection of first-order differential equations is obtained by decomposing the nonlinear differential equations into a set of first-order differential equations. As indicated in the picture, the linked ordinary differential equations (15)-(17) have been reduced to a system of seven simultaneous equations for seven unknowns. The coupled ordinary differential Eqs. (15)-(17) are third order in $f(\eta)$ and second order in $\theta(\eta)$ and ϕ (η) which have been reduced to a system of seven simultaneous equations for seven unknowns. In order to numerically solve this system of equation ns using Runge-Kutta method, the solutions require seven initial conditions but two initial conditions in $f(\eta)$ one initial condition in each of $\theta(\eta)$ and ϕ (η) are known. However, the values of $f'(\eta)$, $\theta(\eta)$ and $\phi(\eta)$ are known at $\eta \to \infty$.

These end conditions are utilized to produce unknown initial conditions at $\eta = 0$ by using shooting technique. The most important step of this scheme is to choose the appropriate finite value of η_∞. Thus to estimate the value of η_∞ we start with some initial guess value and solve the boundary value problem consisting of Eqs. (15)-(17) to obtain $f''(0), \theta'(0)$ and $\phi'(0)$. The solution process is repeated with another larger value of η_∞ until two successive values of $f''(0), \theta'(0)$ and $\phi'(0)$ differ only after desired significant digit. The last value η_∞ is taken as the finite value of the limit η_∞ for the particular set of physical parameters for determining velocity, temperature and concentration, respectively, are $f(\eta)$, $\theta(\eta)$ and ϕ (η) in the boundary layer. After getting all the initial conditions we solve this system of simultaneous equations using fourth order Runge-Kutta integration scheme. The value of η_∞ is selected to 8 depending on the physical parameters governing the flow so that no numerical oscillation would occur. Thus, the coupled boundary value problem of third-order in $f(\eta)$, second-order in $\theta(\eta)$ and ϕ (η) has been reduced to a system of seven simultaneous equations of first-order for seven unknowns as follows:

$$\left.\begin{aligned}
&f' = p \Rightarrow f'' = p' = q \Rightarrow f''' = p'' = q' \\
&\Rightarrow q' = \frac{2p^2 + (M+K)p - fq}{\left(1 + \frac{1}{\beta}\right)} \\
&\theta' = r \Rightarrow \theta'' = r' \text{ then} \\
&r' = -\frac{(\Pr)(Nb)rz + (\Pr)(Nt)r^2 + (\Pr)Hp^2 + (\Pr)fr}{\left(1 + \frac{4R}{3}\right)} \\
&\&\ \phi' = z \Rightarrow \phi'' = z' \text{ then} \\
&z' = \frac{(Nb)\gamma\phi - (Le)(Nb)fz - (Nt)r'}{Nb}
\end{aligned}\right\} \tag{23}$$

and the corresponding boundary conditions became

$$f\left(0\right)=S,\ p\left(0\right)=1+\lambda p'\left(0\right),\ \theta\left(0\right)=1+\delta r\left(0\right),\ \phi\left(0\right)=1,\ p\left(\infty\right)\rightarrow 0,\ \theta\left(\infty\right)\rightarrow 0,\ \phi\left(\infty\right)\rightarrow 0 \quad (24)$$

The boundary value problem is first converted into an initial value problem (IVP), which is then further explored. The beginning value problem is then solved by accurately guessing the missing starting value for various combinations of factors using the shooting method, which is repeated until the problem is solved. In this instance, the step size h = 0.1 is used for calculating purposes. Additionally, a 10^{-6} error tolerance is being used. The information gathered is presented in the form of tables and graphs, with the main features of the problems addressed and explored in depth.

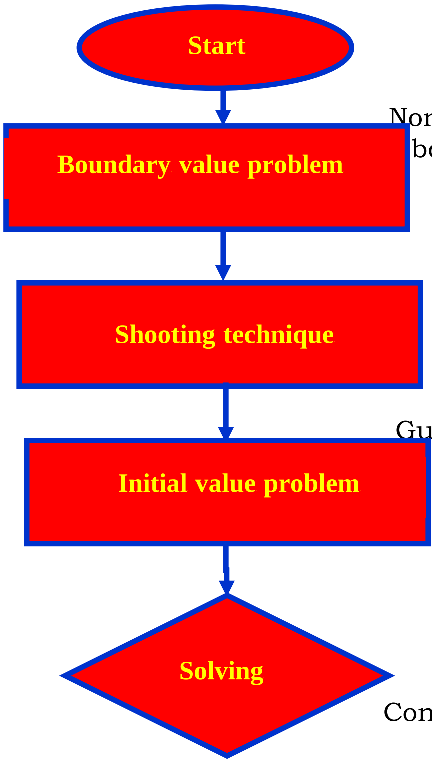

Non-dimensionalization of boundary value problem

Guessing initial condition

R-K Method

Convergence criterion 10^{-8}

Fig. 3. Flow diagram of the numerical procedure

Program Code Validation

Table 1
Comparison of present Nusselt number coefficient results with published results of Rudraswamy and Gireesha [44] and Anand Rao et al. [45]

Pr	Rudraswamy and Gireesha [44]	Anand Rao et al. [45]	Present results
0.72	0.6180	0.6152	0.605882122457898
1.00	0.7097	0.7093	0.695441203154867
1.50	0.7862	0.7862	0.779522102148914

In order to check the validity of current solutions a comparison is carried out between present results and the results given in Rudraswamy and Gireesha [44], Anand Rao et al. [45], Meraj Mustafa et al. [46] and Anuar Ishak [47]. This comparison is shown in the tables 1 and 2 where a fine conformity has noticed in both results and hence ensured the validity of current results.

Table 2
Comparison of present Nusselt number coefficient results with published results of Meraj Mustafa et al. [46] and Anuar Ishak [47]

Pr	Meraj Mustafa et al. [46]	Anuar Ishak [47]	Present results
0.40	0.4619	0.4620	0.458996203178521
0.70	0.6190	0.6192	0.609885102314757
1.00	0.7176	0.7182	0.709885221302658
1.20	0.7581	0.7585	0.748521103447599

Results and Discussion

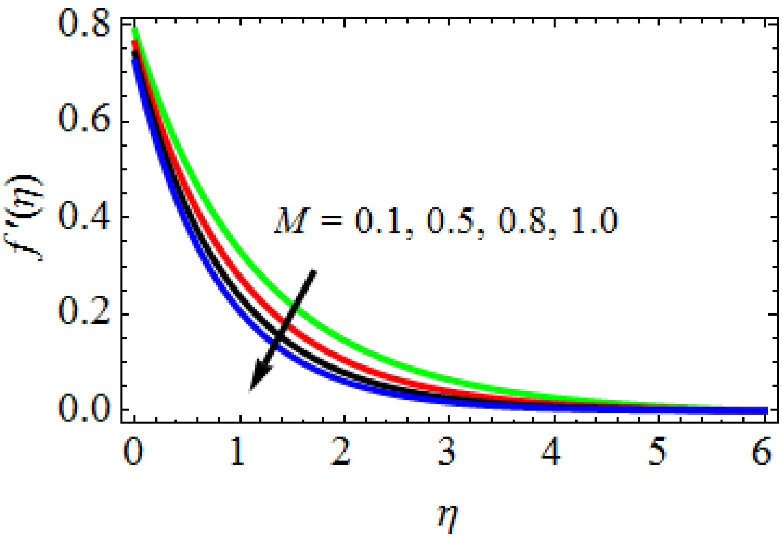

Fig. 4. *M* effect on velocity profiles

In this current work, the combined effects of velocity and thermal slip effects on viscous, electrically, incompressible, Casson and nanofluid flow towards an exponentially stretching sheet in the presence of Chemical reaction, Joule heating, Thermophoresis and Brownian motion effects. The resultant transformed ordinary differential equations (15), (16), and (17) are numerically solved with the necessary boundary conditions (18) using the Runge-Kutta method and the shooting technique. We investigate the effects of the governing physical parameters, namely Magnetic field parameter (M), Casson fluid parameter (β), Permeability parameter (K), Velocity slip parameter (λ), Suction/Injection parameter (S), Prandtl number (Pr), Thermal radiation parameter (R), Brownian motion parameter (Nb), Thermophoresis parameter (Nt), Joule heating parameter (H), Thermal slip parameter (δ), Lewis number (Le) and Chemical reaction parameter (γ) on velocity, temperature, concentration profiles and at the same time the coefficient of skin-friction, Nusselt number, Sherwood number coefficients at the wall are also investigated and illustrated in Figs. 4, 5, 6, 7, 8, 9, 10, 11, 12, 13, 14, 15, 16, 17, 18, 19, 20 and Tables 3, 4, 5 and 6 respectively.

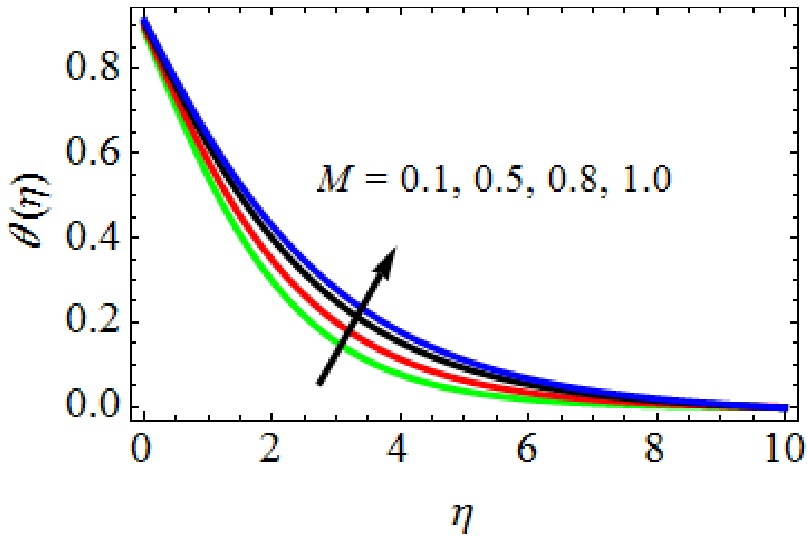

Fig. 5. M effect on temperature profiles

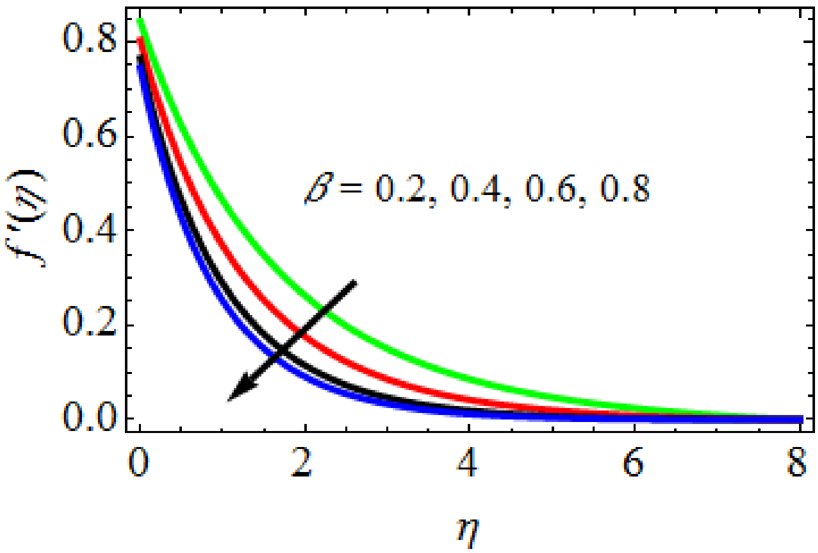

Fig. 6. β effect on velocity profiles

Figs. 4 and 5 illustrate the influence of the magnetic field parameter (M) on velocity and temperature profiles, respectively. Based on these figures, we were able to reduce that the velocity of the fluid dropped as the magnetic field rose by 0.1, 0.5, 0.8, and 1.0; in contrast, the temperature profiles revealed the behaviour of growing as the magnetic field increased. This is because the magnetic field provides what is known as a Lorentz force, which is a decelerating body force that acts in the opposite direction of the direction of the actual magnetic field. Because of this body force, the flow of the boundary layer as well as the thickness of the momentum boundary layer are both reduced. In a similar manner, it generates heat because of the Lorentz force, which is a fractional resistive force that works against the velocity of the fluid. Because of this property, the thermal boundary layer will be greater in thickness when the magnetic field is stronger.

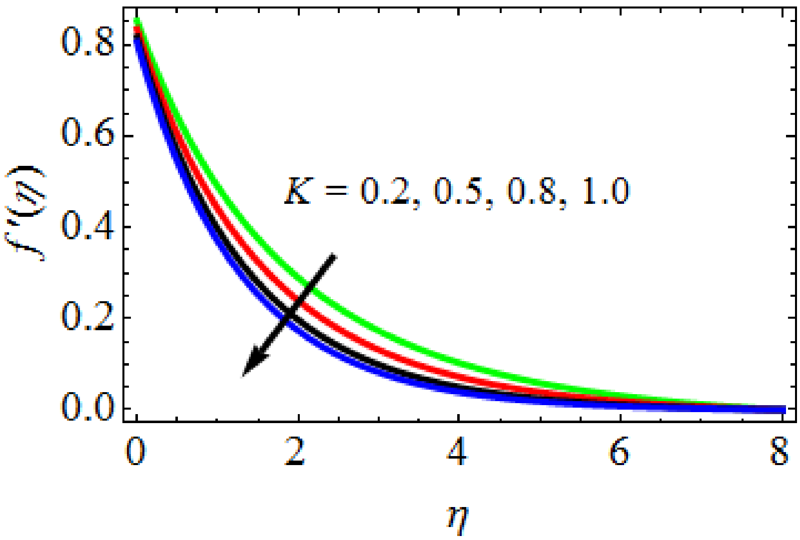

Fig. 7. K effect on velocity profiles

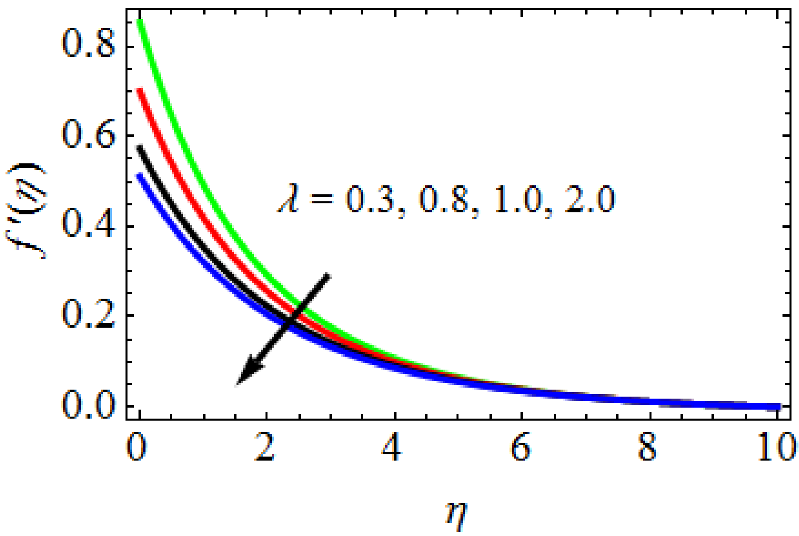

Fig. 8. λ effect on velocity profiles

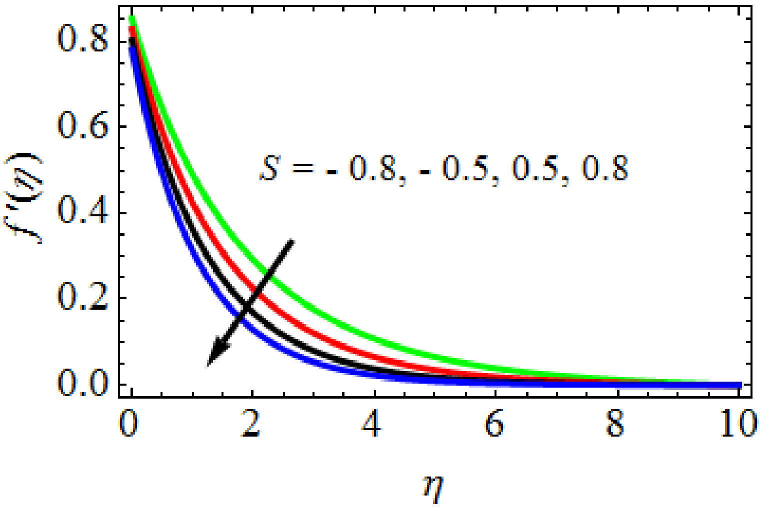

Fig. 9. S effect on velocity profiles

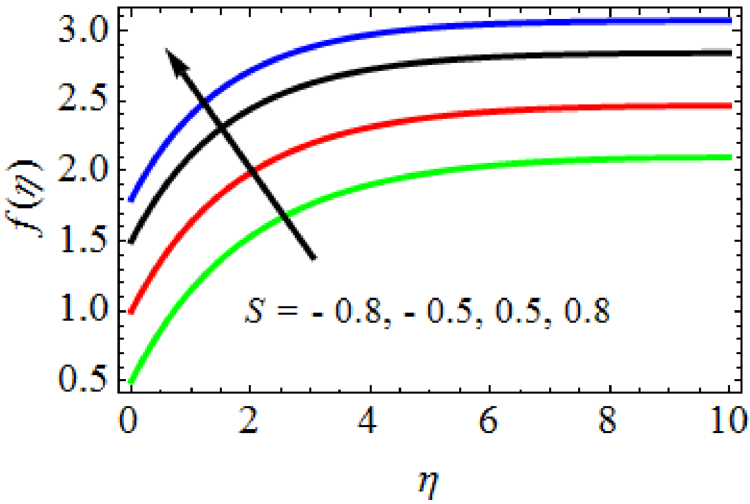

Fig. 10. S effect on streamwise velocity profiles

The impact of some of the physical parameters on velocity profiles are discussed in the form of graphs. Yield stress in Casson nanofluid decreases with an increase in β that increases the magnitude of plastic dynamic viscosity thus greater resistance in the fluid flow is produced. Greater resistance to flow will obviously decrease the velocity of the fluid. This fact is evident from the graphical results in Fig. 6 as an increase in β decreases the fluid velocity. It is possible to observe in Fig. 7 how the Permeability parameter (K) affects the velocity field. We may infer from this graph that when the porosity parameter is increased, the velocity profile decreases in magnitude. Due to the fact that a rise in K magnifies the porous layer, the thickness of the momentum boundary layer is reduced as a result of this. Darcian's body force is responsible for the physical transfer of heat from the solid wall to the flow zone.

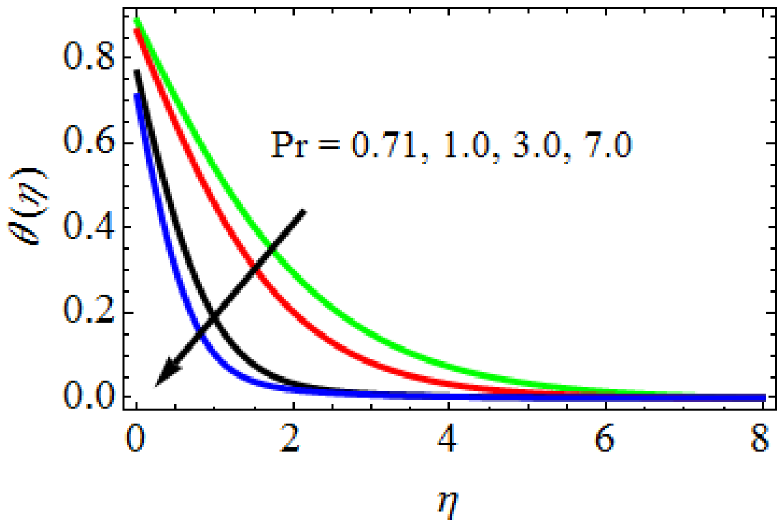

Fig. 11. Pr effect on temperature profiles

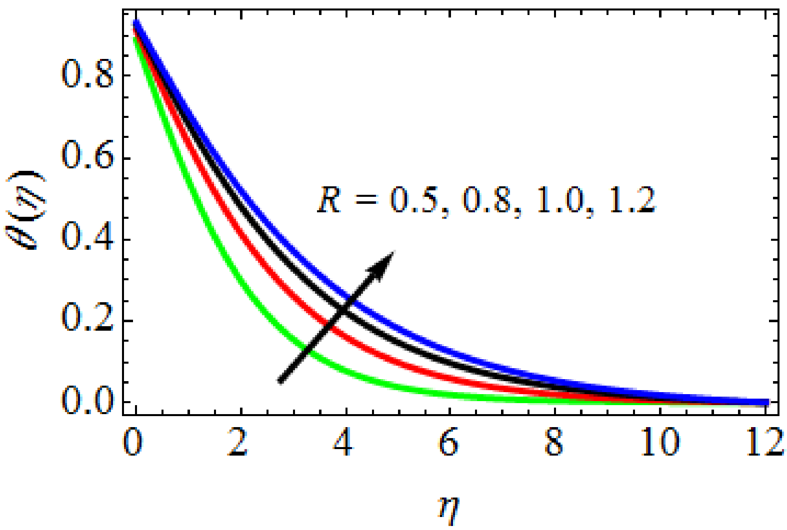

Fig. 12. R effect on temperature profiles

The effect of velocity slip parameter (λ) on velocity profiles is shown in Fig. 8. When the velocity slip parameter is increased, the relative velocities of the stretched sheet and the fluid decrease. Because when the velocity slip parameter is increased, the nanofluid velocity decreases, this is the case. Fig. 9 illustrate the effect of suction/injection parameter (S) on velocity profiles. The suction/injection parameter controls fluid flow. It is easy to discern that for greater values of S velocity (Fig. 9) profile decrease. For $S < 0$ (injection), the fluid nearest the boundary boosts which increases flow velocity and the collision between the molecules, that in turn causes an increase in the internal kinetic energy. On the other hand, for $S > 0$ (suction), the fluid near the boundary is sucked, which creates porosity near the boundary, which in turn reduces the velocity profile. Fig. 10 shows the impact of the suction/injection (S) on the dimensionless velocity profiles $f(\eta)$. The curves in Fig. 10 show that the boundary S altogether affects the thickness of the boundary layer. With rising *S*, the flow appears to decelerate dramatically. The boundary layer adheres more tightly to the wall because of suction/injection. As a result, momentum is lost, resulting in a decrease in velocity. As a result of suction/injection, the thickness of the energy limit layer is decreased.

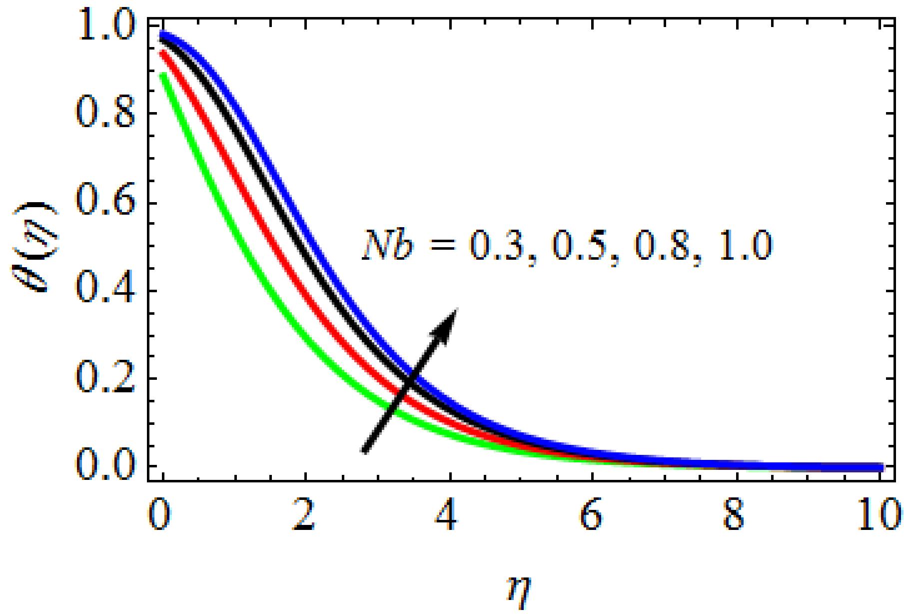

Fig. 13. *Nb* effect on temperature profiles

Fig. 11 presents the effect of Prandtl number (Pr) on the fluid temperature. As the value of Pr increases, the temperature gradient of the fluid decreases. As Pr increases, the momentum diffusivity increases and dominates the thermal diffusivity. The fluid velocity is high enough to help the heat transfer of the fluid. This makes the heat dissipation rate faster and makes the boundary layer to become thinner. In Fig. 12, increase in the temperature profiles are shown by increase in thermal radiation parameter (*R*). Physically, radiative heat transfer is less than conductive heat transfer, which reduces the buoyancy force and thermal boundary layer thickness. Obtained result is a positive proof of the relation of $R = \dfrac{4\sigma^{*} T_{\infty}^{3}}{\kappa K^{*}}$.

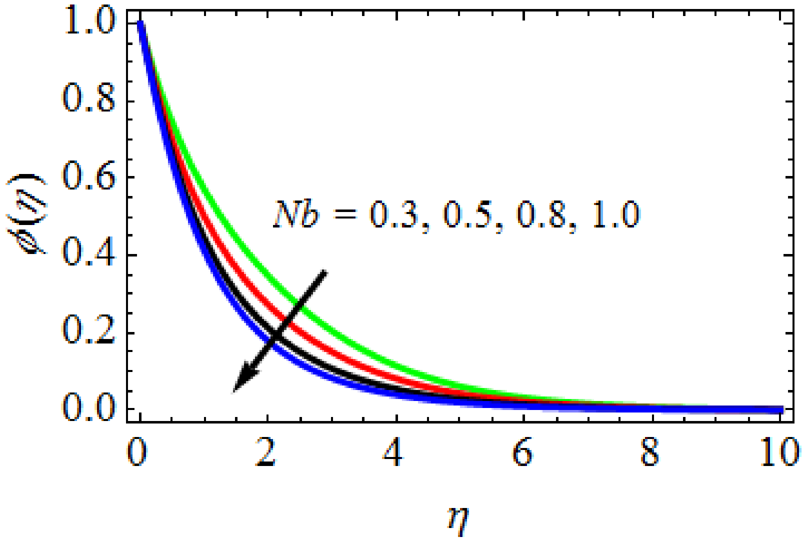

Fig. 14. *Nb* effect on concentration profiles

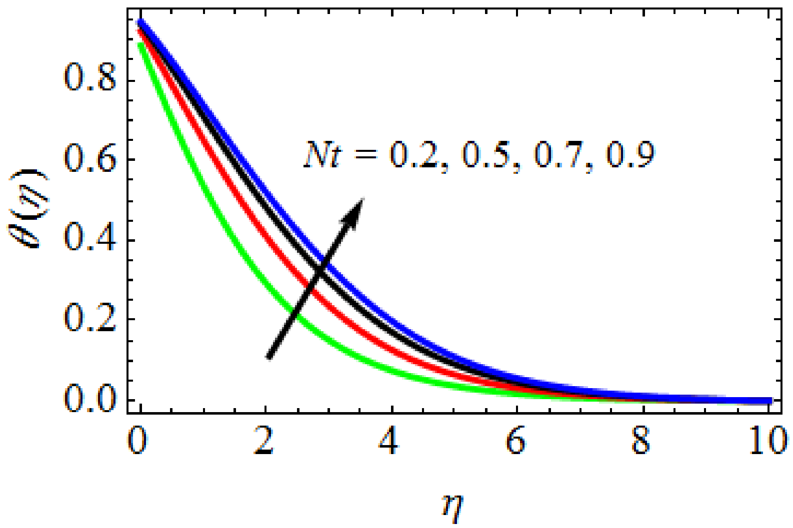

Fig. 15. *Nt* effect on temperature profiles

The effect of the Brownian motion parameter (*Nb*) on temperature and concentration profiles is shown in Figs. 13 and 14 respectively. The temperature profile settled at higher values by an increase in the Brownian motion parameter. Brownian motion is the random motion due to the collisions between nanoparticles and base fluid. More is the Brownian motion parameter; more is the collision. Due to collision between particles, the internal kinetic energy of the fluid increases. There is a reverse relationship between the Brownian motion parameter and concentration profile. More is the Brownian motion parameter; less is the number of nanoparticles in the base fluid.

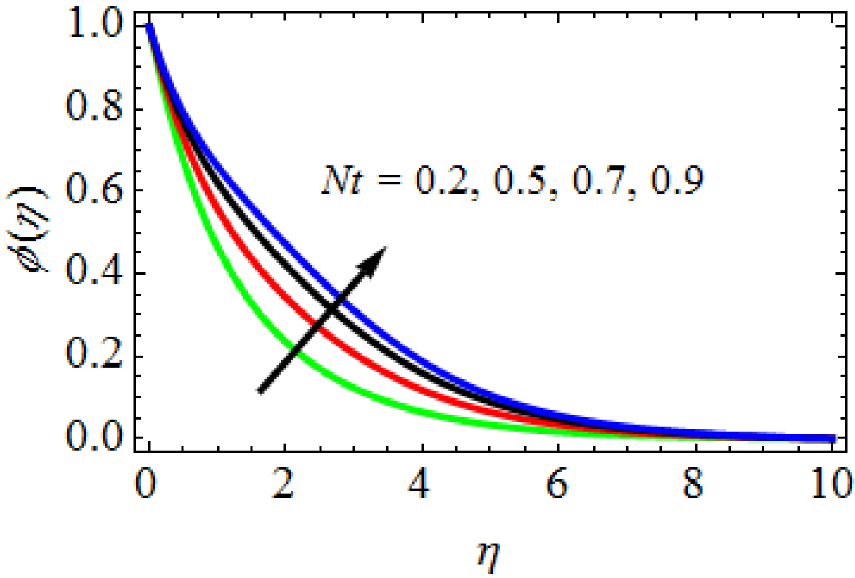

Fig. 16. *Nt* effect on concentration profiles

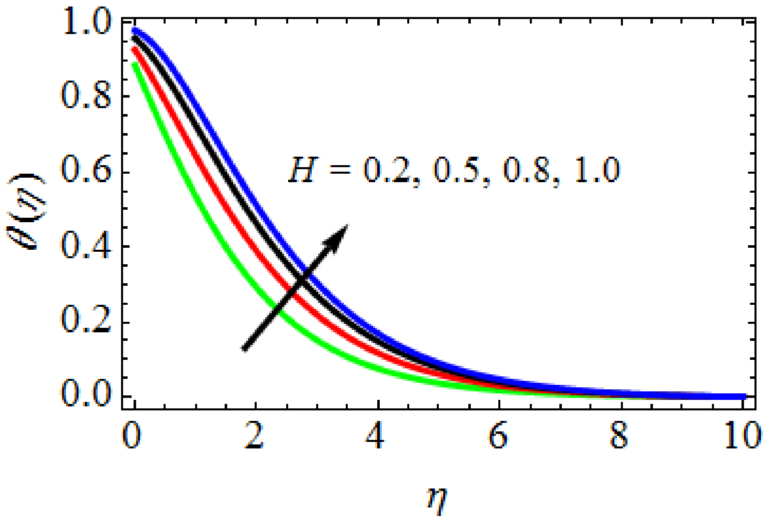

Fig. 17. *H* effect on temperature profiles

Figs. 15 and 16 reveal the impact of thermophoresis parameter (*Nt*) on temperature and concentration profiles. Both temperature and concentration profiles increase for higher values of *Nt*. Thermophoresis is the transport force that occurs due to the temperature gradient between layers of the fluid. More Thermophoresis parameter means that the temperature difference between the layer increases, so the heat transformation rate also increases. By increasing the nanoparticles, the concentration of the fluid increases. More is the nanoparticles more is the heat transformation between the layers, so *Nt* increases both temperature profiles as well as concentration profiles. As shown in Fig. 17, it is observed that an increase in joule heating parameter (*H*) the profiles for temperature are decreasing. Fig. 18 exhibits the effect of the thermal slip parameter (δ) on the dimensionless temperature profiles. It is clearly shown that by increasing the values of δ, the temperature profiles are decreases. As the value of the thermal slip parameter increases, the thermal boundary layer thickness decreases even when a small amount of heat is transferred to the fluid from the sheet.

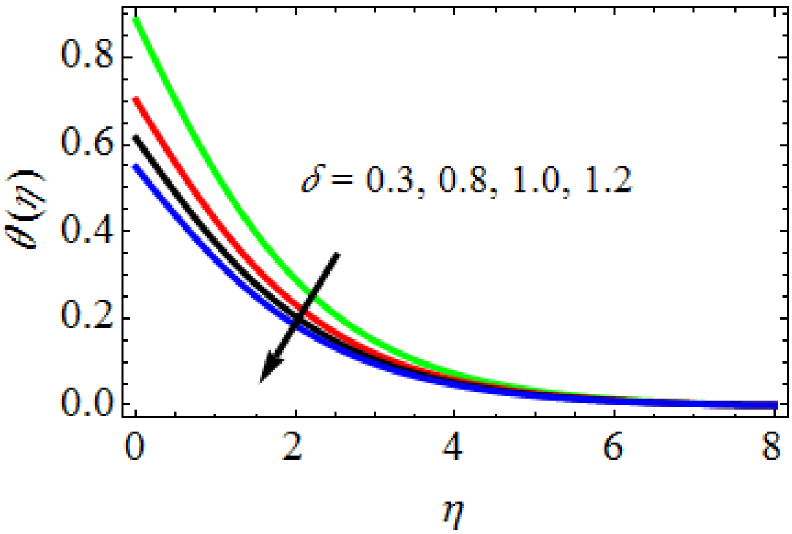

Fig. 18. δ effect on temperature profiles

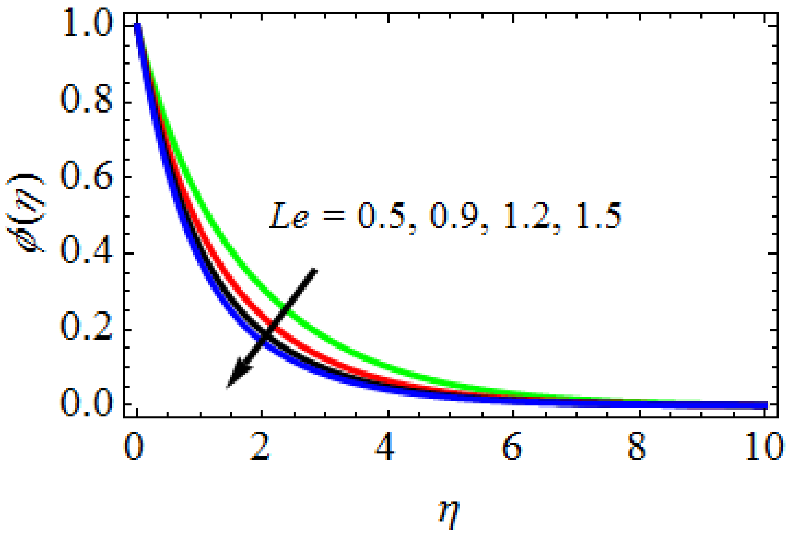

Fig. 19. Le effect on concentration profiles

Fig. 19 shows the effect of Lewis number (Le) on the dimensionless concentration for fixed values of other parameters. It is observed that for larger values of Le suppress the concentration profile *i.e.* inhibit nanoparticle species diffusion, as observed. There will be a much greater reduction in the concentration boundary layer thickness. The effect of increasing the reaction rate parameter (γ) on the species concentration profiles for generative chemical reaction is shown in Fig. 20.

It is noticed from this graph that there is marked effect of increasing the value of the chemical reaction rate parameter γ on concentration distribution in the solutal boundary layer. It is clearly observed from this figure that the value of the concentration of species at start of the boundary layer decreases till it attains the minimum value of zero at the end of the boundary layer and this trend is seen for all the values of reaction rate parameter. Further, it is observed that increasing the value of the chemical reaction rate parameter decreases the concentration of species in the boundary layer, this is due to the fact that solutal boundary layer decreases with γ.

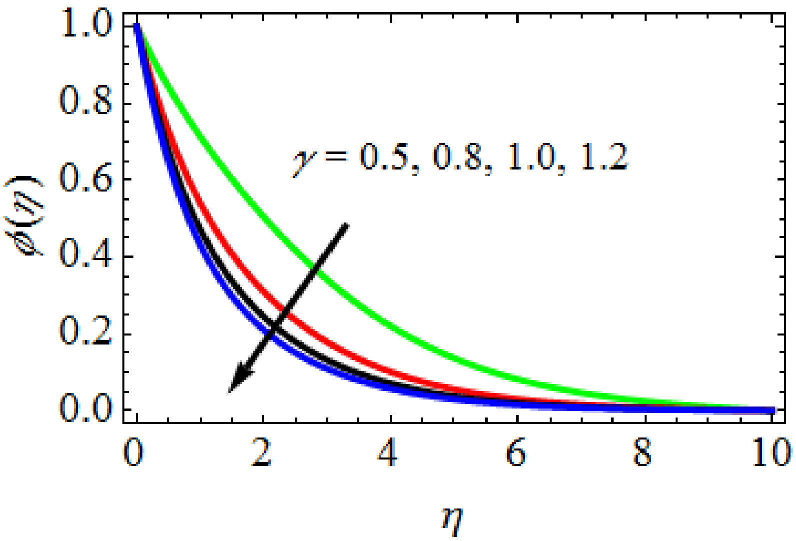

Fig. 20. γ effect on concentration profiles

Table-3 and Table-4 show the numerical values of Skin-friction coefficient for variations in values of the engineering parameters such as, Magnetic field parameter (M), Casson fluid parameter (β), Permeability parameter (K), Velocity slip parameter (λ), Suction/Injection parameter (S), Prandtl number (Pr), Thermal radiation parameter (R), Brownian motion parameter (Nb), Thermophoresis parameter (Nt), Joule heating parameter (H), Thermal slip parameter (δ), Lewis number (Le) and Chemical reaction parameter (γ). From this table, it is observed that the Skin-friction coefficient is increasing with rising values of Thermal radiation parameter (R), Brownian motion parameter (Nb), Thermophoresis parameter (Nt), Joule heating parameter (H), while it is decreasing with increasing values of Magnetic field parameter (M), Casson fluid parameter (β), Permeability parameter (K), Velocity slip parameter (λ), Suction/Injection parameter (S), Prandtl number (Pr), Thermal slip parameter (δ), Lewis number (Le) and Chemical reaction parameter (γ).

The numerical values of rate of heat transfer coefficient in terms of Nusselt number are displayed in Table-5 for different values of Magnetic field parameter (M), Prandtl number (Pr), Thermal radiation parameter (R), Brownian motion parameter (Nb), Thermophoresis parameter (Nt), Joule heating parameter (H) and Thermal slip parameter (δ). The rate of heat transfer coefficient is gradually rising with increasing values of Magnetic field parameter (M), Thermal radiation parameter (R), Brownian motion parameter (Nb), Thermophoresis parameter (Nt), Joule heating parameter (H), while the reverse effect is observed in increasing values of Prandtl number (Pr) and Thermal slip parameter (δ). The effects of Brownian motion parameter (Nb), Thermophoresis parameter (Nt), Lewis number (Le) and Chemical reaction parameter (γ) on rate of mass transfer coefficient or in terms Sherwood number coefficient are discussed in Table-6. From this table, it is observed that the rate of mass transfer coefficient is increasing with increasing values of Thermophoresis parameter (Nt) and decreasing with increasing values of Brownian motion parameter (Nb), Lewis number (Le) and Chemical reaction parameter (γ).

Table 3

Numerical values of Skin-friction coefficient for variations of M, β, K, λ, S, Pr and R

M	β	K	λ	S	Pr	R	Cf
0.1	0.2	0.2	0.3	- 0.8	0.71	0.5	1.962001542180248
0.5							1.874159521466023
0.8							1.849647976987932
	0.4						1.926379874979958
	0.6						1.904768795844385
		0.5					1.905665930490505
		0.8					1.886789585938498
			0.8				1.927675498766976
			1.0				1.897875984649856
				- 0.5			1.906789729875845
				0.5			1.877956942907408
				0.8			1.856789474996529
					1.0		1.888984739847646
					3.0		1.848838764876099
						0.8	1.998883284208287
						1.0	2.043848006982492

Table 4

Numerical values of Skin-friction coefficient for variations of Nb, Nt, H, δ, Le and γ

Nb	Nt	H	δ	Le	γ	Cf
0.3	0.2	0.2	0.3	0.5	0.5	1.962001542180248
0.5						2.076598479846574
0.8						2.123484967398393
	0.5					2.056747476982489
	0.7					2.138897494984294
		0.5				1.989865847656420
		0.8				2.057894796438394
			0.8			1.903464874867579
			1.0			1.876784987456502
				0.9		1.935878734467209
				1.2		1.902987587299283
					0.8	1.927858448979244

					1.0	1.896787498748393

Table 5
Numerical values of rate of heat transfer coefficient for variations of *M*, Pr, *R*, *Nb*, *Nt*, δ and *H*

M	Pr	*R*	*Nb*	*Nt*	δ	*H*	*Nu*
0.1	0.71	0.5	0.3	0.2	0.3	0.2	0.456590267456824
0.5							0.487874827984729
0.8							0.505876982742984
	1.0						0.416926964298572
	3.0						0.365652076563799
		0.8					0.489687498259383
		1.0					0.519892348794768
			0.5				0.490959872984573
			0.8				0.522854398298641
				0.5			0.509492690238209
				0.7			0.532843987420902
					0.8		0.417984892498297
					1.0		0.391734706239669
						0.5	0.478509209958731
						0.8	0.499387597230937

Table 6
Rate of mass transfer coefficient values for different values of *Le*, *Nb*, γ and *Nt*

Le	*Nb*	γ	*Nt*	*Sh*
0.5	0.3	0.5	0.2	0.594679479426894
0.9				0.557697348738753
1.2				0.528478472603847
	0.5			0.556749874457485
	0.8			0.522239699863876
		0.8		0.560869823690748
		1.0		0.541776237743630
			0.5	0.622876446582373
			0.7	0.656584376764837

Conclusions

Numerical analysis of viscous, incompressible, electrically conducting Casson-nanofluid over a non-linearly stretching sheet surrounded by porous medium with velocity, thermal slip boundary conditions subject to magnetic field and Joule heating was studied in the present article. The transformed ordinary differential equations were solved using an efficient Runge-Kutta method along with shooting technique. For this flow, the effects of some important physical parameters on the velocity, temperature and concentration profiles were analyzed in form of graphs. Also, the numerical values of Skin-friction coefficient, Nusselt and Sherwood numbers were also calculated to observe the Casson-nanofluid phenomena for the present model. Some of the important findings in the study can be summarized in the following points.

- The velocity profiles are increasing with rising values of Thermal radiation parameter (R), Brownian motion parameter (Nb), Thermophoresis parameter (Nt), Joule heating parameter (H).
- The velocity profiles are decreasing with increasing values of Magnetic field parameter (M), Casson fluid parameter (β), Permeability parameter (K), Velocity slip parameter (λ), Suction/Injection parameter (S), Prandtl number (Pr), Thermal slip parameter (δ), Lewis number (Le) and Chemical reaction parameter (γ).
- The temperature profiles are rising with increasing values of Magnetic field parameter (M), Thermal radiation parameter (R), Brownian motion parameter (Nb), Thermophoresis parameter (Nt), Joule heating parameter (H).
- The temperature profiles are falling with increasing values of Prandtl number (Pr) and Thermal slip parameter (δ).
- The concentration profiles are growing with rising values of Thermophoresis parameter (Nt) and the reverse effect is observed with increasing values of Brownian motion parameter (Nb), Lewis number (Le) and Chemical reaction parameter (γ).
- An increase in Nt appreciably enhances the mass flux due to temperature gradient which in turn raises the nanoparticles concentration.
- The impact of chemical reaction and thermal radiation in the presence of uniform thermophoresis and Brownian diffusion motion has a substantial effect on flow field.
- The present results are in good achieved in this work are more comprehensive form of Rudraswamy and Gireesha [44], Anand Rao et al. [45], Meraj Mustafa et al. [46] and Anuar Ishak [47].

References

1. R. Kandasamy, I. Muhaimin, R. Mohamad, Thermophoresis and Brownian motion effects on MHD boundary-layer flow of a nanofluid in the presence of thermal stratification due to solar radiation, International Journal of Mechanical Sciences, 70 (2013), pp. 146-154.
2. G. Herdrich, M. Auweter-Kurtz, M. Fertig, A. Nawaz, D. Petkow, MHD flow control for plasma technology applications, Vacuum, 80 (2006), pp. 1167-1173.
3. Veera Krishna, M., Ameer Ahammad, N. and Chamkha, A. J., 2021. Radiative MHD flow of Casson hybrid nanofluid over an infinite exponentially accelerated vertical porous surface, *Case Studies in Thermal Engineering*, *27*, pp. 101229.
4. Veera Krishna, M. and Chamkha, A. J., 2019. Hall and ion slip effects on MHD rotating boundary layer flow of nanofluid past an infinite vertical plate embedded in a porous medium. *Results in Physics*, *15*, pp. 102652.
5. Veera Krishna, M. and Chamkha, A. J., 2020. Hall and ion slip effects on MHD rotating flow of elastico-viscous fluid through porous medium. *International Communications in Heat and Mass Transfer*, *113*, pp. 104494.

6. Veera Krishna, M., Jyothi, K. and Chamkha, A. J., 2020. Heat and mass transfer on MHD flow of second-grade fluid through porous medium over a semi-infinite vertical stretching sheet. *Journal of Porous Media*, *23*(8), pp. 751-765.
7. Veera Krishna, M. and Chamkha, A. J., 2019. Hall effects on MHD Squeezing flow of a water based nano fluid between two parallel disks. *Journal of Porous Media*, *22*(2), pp. 209-223.
8. Veera Krishna, M., Anand, P. V. S. and Chamkha, A. J., 2019. Heat and mass transfer on Free convective flow of a micropolar fluid through a porous surface with inclined magnetic field and Hall effects. *Special Topics and Reviews in Porous Media: An International Journal*, *10*(3), pp. 203-223.
9. Veera Krishna, M. and Chamkha, A. J., 2019. MHD Peristaltic Rotating Flow of a Couple Stress Fluid through a Porous Medium with Wall and Slip effects. *Special Topics and Reviews in Porous Media: An International Journal*, *10*(3), pp. 245-258.
10. Veera Krishna, M., Subba Reddy, G. and Chamkha, A. J., 2018. Hall effects on unsteady MHD oscillatory free convective flow of second grade fluid through porous medium between two vertical plates. *Physics of Fluids*, *30*(2), pp. 023106.
11. Veera Krishna, M. and Chamkha, A. J., 2018. Hall effects on unsteady MHD flow of second grade fluid through porous medium with ramped wall temperature and ramped surface concentration. *Physics of Fluids*, *30*(5), pp. 053101.
12. Veera Krishna, M., Jyothi, K. and Chamkha, A. J., 2018. Heat and mass transfer on unsteady, magnetohydrodynamic, oscillatory flow of second-grade fluid through a porous medium between two vertical plates, under the influence of fluctuating heat source/sink, and chemical reaction. *International Journal of Fluid Mechanics Research*, *45*, pp. 459-477.
13. Veera Krishna, M., Swarnalathamma, B. V. and Chamkha, A. J., 2018. Heat and mass transfer on magnetohydrodynamic chemically reacting flow of micropolar fluid through a porous medium with Hall effects. *Special Topics and Reviews in Porous Media: An International Journal*, *9*(4), pp. 347-364.
14. Veera Krishna, M., Bharathi, K. and Chamkha, A. J., 2018. Hall effects on MHD Peristaltic flow of Jeffrey fluid through porous medium in a vertical stratum. *Interfacial Phenomena and Heat Transfer*, *6*(3), pp. 253-268.
15. Krishna, M. V. and Chamkha, A. J., 2020. Hall and ion slip effects on Unsteady MHD Convective Rotating flow of Nanofluids-Application in Biomedical Engineering. *Journal of Egyptian Mathematical Society*, *28* (1), https://doi.org/10.1186/s42787-019-0065-2.
16. ThameemBasha, H., Sivaraj, R., Subramanyam Reddy, A. and Chamkha, A. J., 2019. SWCNH/diamond-ethylene glycol nano-fluid flow over a wedge, plate and stagnation point with induced magnetic field and non-linear radiation-solar energy application. *The European Physical Journal Special Topics*, *228*, pp. 2531-2551.
17. Kumar, B., Seth, G. S., Nandkeolyar, R. and Chamkha, A. J., 2019. Outlining the impact of induced magnetic field and thermal radiation on magneto-convection flow of dissipative fluid. *International Journal of Thermal Sciences*, *146*, pp. 106101.
18. Modather, M., Rashad, A. M. and Chamkha, A. J., 2009. An analytical study of MHD heat and mass transfer oscillatory flow of a micropolar fluid over a

vertical permeable plate in a porous medium. *Turkish Journal of Engineering and Environmental Sciences*, *33*, pp. 245-257.

19. Sudarsana Reddy, P., Sreedevi, P. and Chamkha, A. J., 2017. MHD boundary layer flow, heat and mass transfer analysis over a rotating disk through porous medium saturated by Cu-water and Ag-water nano-fluid with chemical reaction. *Powder Technology*, *307*, pp. 46-55.
20. Ramesh, G. K., Shehzad, S. A., Rauf, A. and Chamkha, A. J., 2020. Heat transport analysis of aluminum alloy and magnetite graphene oxide through permeable cylinder with heat source/sink. *PhysicaScripta*, *95*(9), pp. 095203, DOI: 10.1088/1402-4896/aba5af.
21. Menni, Y., Chamkha, A. J., Massarotti, N., Ameur, H., Kaid, N. and Bensafi, M., 2020. Hydrodynamic and thermal analysis of water, ethylene glycol and water-ethylene glycol as base fluids dispersed by aluminum oxide nano-sized solid particles. *International Journal of Numerical Methods for Heat and Fluid Flow*, *30*(9), pp. 4349-4386.
22. Ganesh Kumar, K., Gnaneswara Reddy, M., Sudharani, M. V. V. N. L., Shehzad, S. A. and Chamkha, A. J., 2020. Cattaneo-Christov heat diffusion phenomenon in Reiner-Philippoff fluid through a transverse magnetic field. *Physica A: Statistical Mechanics and its Applications*, *541*, pp. 123330.
23. B. C. Sakiadis, Boundary layer behaviour on a continuous solid surface: boundary layer equations for two dimensional and axi-symmetric flow, AIChE J., 7 (1961), pp. 26-28.
24. A. Mamun, A. Arifuzzaman, Sk. R.E. Rabbi, Numerical simulation of periodic MHD casson nanofluid flow through porous stretching sheet, SN Appl. Sci., 3 (2021), p. 271, 10.1007/s42452-021-04140-3.
25. Z. Shah, P. Kumam, and W. Deebani, Radiative MHD Casson nanofluid flow with activation energy and chemical reaction over past nonlinearly stretching surface through entropy generation. Sci. Rep. 10, 1–14 (2020).
26. M. K. Nayak, A. K. A. Hakeem, B. Ganga, M. I. Khan, M. Waqas, O. D. Makinde, Entropy optimized MHD 3D nanomaterial of non-Newtonian fluid: a combined approach to good absorber of solar energy and intensification of heat transport, Comput. Methods Progr. Biomed., 186 (2020), Article 105131,
27. G. Rasoola, A. J. Chamkha, T. Muhammad, A. Shafiqd, I. Khan, Darcy-Forchheimer relation in Casson type MHD nanofluid flow over non-linear stretching surface, Propulsion and Power Res., 9 (2) (2020), pp. 159-168, 10.1016/j.jppr.2020.04.003.
28. A. Kamran, S. Hussain, M. Sagheer, N. Akmal, A numerical study of magnetohydrodynamics flow in Casson nanofluid combined with Joule heating and slip boundary conditions, Res. Phys., 7 (2017), pp. 3037-3048.
29. C. Sulochana, G. P. Ashwinkumar and N. Sandeep, (2016). Similarity solution of 3D Casson nanofluid flow over a stretching sheet with convective boundary conditions. J. Niger. Math. Soc., Vol. 35, pp. 128-141.
30. J. Raza, Thermal radiation and slip effects on magnetohydrodynamic (MHD) stagnation point flow of Casson fluid over a convective stretching sheet, Propul. Power Res., Vol. 8 (2019) pp. 138-146.
31. P.V. Kumar, S.M. Ibrahim, G. Lorenzini, The study of three dimensional radiative MHD casson nanofluid over an exponential porous stretching sheet with heat source under convective boundary conditions, Int. J. Heat Technol., 36 (2018) 1-10.

32. I. Ullah, S. Shafie, I. Khan, Effects of slip condition and Newtonian heating on MHD flow of Casson fluid over a nonlinearly stretching sheet saturated in a porous medium, J. King Saud Univ. Sci. 29 (2016) 250-259.
33. B. Souayeh, M.G. Reddy, P. Sreenivasulu, T. Poornima, M.R. Gorji, I.M. Alarifi, Comparitive analysis on non-linear radiative heat transfer on MHD Casson nanofluid past a thin needle, J. Mol. Liq. 284 (2019) 163-174.
34. M. M. Rashidi, N. Vishnu Ganesh, A. K. Abdul Hskeem, B. Ganga, Buoyancy effect on MHD flow of nanofluid over a stretching sheet in presence of thermal radiation, J. Mol. Liq. 198 (2014), pp. 234-238.
35. S. Shaw, A. Patra, A. Misra, M. K. Nayak, A. J. Chamkha, A numerical approach to the modeling of thomson and troian slip on nonlinear radiative microrotation of Casson Carreau nanomaterials in magnetohydrodynamics, J. Nanofluid, 10 (3) (2021), pp. 305-315.
36. G. Mahanta, M. Das, M. K. Nayak, S. Shaw, Irreversibility analysis of 3D magnetohydrodynamic Casson nanofluid flow past through two bi-directional stretching surfaces with nonlinear radiation, J. Nanofluids, 10 (2021), pp. 316-326.
37. J. A. Gbadeyan, E. O. Titiloye, A. T. Adeosun, Effect of variable thermal conductivity and viscosity on Casson nanofluid flow with convective heating and velocity slip, Heliyon, 6 (2020), Article e03076.
38. T. Hayat, S. Asad, A. Alsaedi, Flow of Casson fluid with nanoparticles, Appl. Math. Mech., 37 (2016), pp. 459-470.
39. M. Archana, B. J. Gireesha, B. C. Prasannakumara, R. S. R. Gorla, Influence of nonlinear thermal radiation on rotating flow of Casson nanofluid, 7 (2) (2017), pp. 91-101, 10.1515/nleng-2017-0041
40. M. Mustafa, J. Ahmad Khan, Model for flow of Casson nanofluid past a non-linearly stretching sheet considering magnetic field effects, AIP Adv., 5 (7) (2015), Article 077148.
41. B. J. Gireesha, M. R. Krishnamurthy, B. C. Prasannakumara, R. S. R. Gorla, MHD flow and nonlinear radiative heat transfer of a Casson nanofluid past a nonlinearly stretching sheet in the presence of chemical reaction, Nanoscience and Technology: An International Journal, 9 (3) (2018), pp. 207-229, 10.1615/NanoSciTechnolIntJ.2018020102.
42. K. Jayarami Reddy, N. P. Madhusudhana, K. Ramakrishna, MHD mixed convection flow of radiating and chemically reactive Casson nanofluid over a nonlinear permeable stretching sheet with viscous dissipation and heat source, Multidiscip. Model. Mater. Struct., 14 (3) (2018), pp. 609-630, 10.1108/MMMS-10-2017-0127.
43. M. Q. Brewster, Thermal Radiative Transfer Properties, John Wiley and Sons, New York (1972).
44. Rudraswamy, N.G. and Gireesha, B.J. (2014) Influence of Chemical Reaction and Thermal Radiation on MHD Boundary Layer Flow and Heat Transfer of a Nanofluid over an Exponentially Stretching Sheet. Journal of Applied Mathematics and Physics, 2, 24-32. http://dx.doi.org/10.4236/jamp.2014.22004.
45. Rao, J. A., Vasumathi, G. and Mounica, J. (2015) Joule Heating and Thermal Radiation Effects on MHD Boundary Layer Flow of a Nanofluid over an Exponentially Stretching Sheet in a Porous Medium. World Journal of Mechanics, 5, 151-164. http://dx.doi.org/10.4236/wjm.2015.59016.

46. M. Mustafaa, T. Hayat and S. Obaidat, Boundary Layer Flow of a Nanofluid over an Exponentially Stretching Sheet with Convective Boundary Conditions, International Journal of Numerical Methods for Heat and Fluid Flow, Vol. 23, No. 6, 2013, pp. 945-959. http://dx.doi.org/10.1108/HFF-09-2011-0179.
47. A. Ishak, MHD Boundary Layer Flow Due to an Exponentially Stretching Sheet with Radiation Effect, Sains Malaysiana, Vol. 40, No. 4, 2011, pp. 391-395.
48. Suryasa, I. W., Rodríguez-Gámez, M., & Koldoris, T. (2021). Get vaccinated when it is your turn and follow the local guidelines. *International Journal of Health Sciences*, *5*(3), x-xv. https://doi.org/10.53730/ijhs.v5n3.2938
49. Suryasa, I. W., Rodríguez-Gámez, M., & Koldoris, T. (2021). Health and treatment of diabetes mellitus. *International Journal of Health Sciences*, *5*(1), i-v. https://doi.org/10.53730/ijhs.v5n1.2864
50. Yuriah, S., Kartini, F., & Isnaeni, Y. (2022). Experiences of women with preeclampsia. International Journal of Health & Medical Sciences, 5(3), 201-210. https://doi.org/10.21744/ijhms.v5n3.1901